THE JOURNAL OF PHYSICAL CHEMISTRY C

Article

pubs.acs.org/JPCC

Supercritical Carbon-Dioxide-Assisted Deposition of Pt Nanoparticles on Graphene Sheets and Their Application as an Electrocatalyst for Direct Methanol Fuel Cells

Jian Zhao,*[,†,‡,§] Liqing Zhang,[†,‡,§] Tao Chen,[∥] Hui Yu,[†,‡,§] Lin Zhang,[†,‡,§] Hao Xue,[†,‡,§] and Haiqing Hu[†,‡,§]

[†]Key Laboratory of Rubber-Plastics Ministry of Education/Shandong Provincial Key Laboratory of Rubber-Plastics, Qingdao University of Science & Technology, China 266042

[‡]Key Laboratory of Organosilicon Chemistry and Material Technology of Ministry of Education, Hangzhou Normal University, Hangzhou, China 31001

[§]Key Laboratory of Molecular Engineering of Polymers of Ministry of Education, Fudan University, Shanghai, China 200433

[∥]School of Chemistry and Chemical Engineering, Yangzhou University, Yangzhou, China 225002

ABSTRACT: A combination of graphene with metal particles is particularly attractive due to the enhanced performance of the hybrid materials. However, direct loading of uniform metal nanoparticles such as Pt on graphene remains a challenge due to the hydrophobic nature of graphene. We herein demonstrate that Pt nanoparticles with uniform size and high dispersion were deposited on graphene surfaces via a facile and efficient supercritical fluid method. The graphene sheets used in this work were produced by rapid thermal expansion of graphite oxide. With the help of supercritical carbon dioxide (SC CO_2), Pt nanoparticles with a mean size of 3.28 nm are evenly distributed on graphene upon the reduction of an organic platinum precursor. The electrocatalytic investigations reveal that the current density of methanol electrooxidation with the resultant Pt/graphene catalyst was ~3.5 times as large as that observed with conventional Pt/carbon black (Vulcan XC-72) catalyst. The results demonstrate that graphene serves as an excellent electrocatalytic carrier, and the supercritical fluid strategy is powerful and promising for the synthesis of highly active electrocatalysts for direct methanol fuel cells.

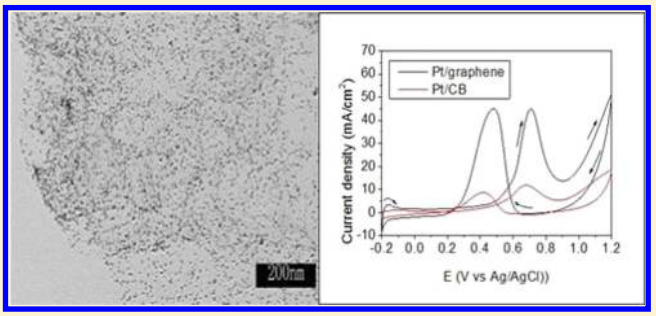

INTRODUCTION

Because of their ease of handling, high energy-conversion efficiency and low operating temperatures, direct methanol fuel cells (DMFCs) are considered to be an attractive power source with potential applications in a variety of systems, ranging from automobiles to portable electronic devices.[1−8] Pt catalysts are regarded as the most popular and effective electrocatalysts for DMFCs. A suitable carbon support is required to immobilize Pt particles to maximize the electrocatalytic activity of Pt and lower the usage of precious Pt. Several forms of carbon materials have been investigated as effective catalyst supports for DMFCs, such as XC-72 carbon black (CB), carbon nanotubes (CNTs), carbon nanofibers (CNFs), and so on.[9−11] Recently, graphene, a 2D atomically thick crystal with carbon atoms arranged in a honeycomb lattice, attracted tremendous scientific and technological interests because of its potential applications in widespread fields.[12−15] The unique properties of graphene, especially high electronic conductivity, huge surface area, mechanical, and thermal stability and durability, make it an attractive 2D support to load precious metals for fuel cell applications.[16,17]

To date, hybrid graphene-supported Pt and alloy elecrocatalysts have been generated by many approaches including impregnation, chemical reduction, electrodeposition methods and so on.[16−22] In general approaches, graphite oxide (GO) was employed as the starting material because the abundant oxygen-containing functional groups of GO enable the solubilization of oxidized graphene sheets and thus allow for the intercalation of molecules such as metal precursors into the interlayer space of GO.[22,23] However, the simultaneous or subsequent reduction of GO (with metal ions) is required, which makes the preparation processes suffer from several disadvantages such as more complex and time-consuming preparation processes as well as excessive and highly toxic reducing reagents that could contaminate graphene flakes.

Rapid thermal expansion of GO is considered to be a promising method for the large-scale production of graphene because graphene sheets can be produced in bulk quantities, the equipment is simple, and the preparation cycle is short and

Received: June 23, 2012
Revised: August 27, 2012
Published: October 2, 2012

requires no post-treatment. Reduction and exfoliation of GO occurs through the evolution of carbon dioxide generated by heating GO in an inert environment. However, because of the hydrophobic properties of graphene sheets, the fabrication methods that made use of the abundant functional groups on GO are not applicable to generating graphene-based metallic catalysts. To load uniformly metal nanoparticles, the employment of surfactants or the functionalization of graphene, which often deteriorates the properties of graphene, has to be involved.[24−27] It is needed to explore novel and simple synthesis methods to immobilize uniform metal nanoparticles directly on the hydrophobic surface of graphene.

Here we demonstrate a facile and effective approach to synthesize Pt nanoparticles uniformly dispersed on graphene. The key is the introduction of supercritical fluid (SCF). The use of SCFs is a rapid, direct, and clean approach to develop nanomaterials and nanocomposites due to its low viscosity, high diffusivity, near zero surface tension, and pressure-dependent density.[28−31] These unique features enable the molecules carried by SCFs to reach to areas with high aspect ratios and poorly wettable substrates. Among all SCFs, supercritical CO_2 (SC CO_2) could be used as a kind of environmentally benign solvent to replace hazardous and volatile organic solvents owing to it being nontoxic, inexpensive, nonflammable, and natural abundant. In recent investigations, Pd, Pt, and Ru nanoparticles were deposited on carbon materials in SCFs by the reduction of organic[11,29] or inorganic metal precursors,[30,31] respectively.

In this work, we exploit SC CO_2 to synthesize high-efficiency Pt/graphene composites successfully upon the hydrogen reduction of platinum(II) acetylacetonate precursor. Graphene used here was produced by rapid thermal expansion of GO. This SCF method is not only suitable for graphene sheets synthesized by rapid thermal expansion but also extendable to graphene with more complicated or inert surfaces. The prepared Pt/graphene nanocomposites were characterized by transmission electron microscopy (TEM), X-ray diffraction (XRD), and X-ray photoelectron spectroscopy (XPS). The electroactive performance of the composites was evaluated at room temperature using electrochemical methods such as cyclic voltammetry (CV) and chronoamperometry (CA) and compared with Pt/carbon black (Vulcan XC-72) composites. The presence of SC CO_2 leads to highly dense and homogeneous deposition of Pt nanoparticles on graphene surfaces. The SCF fabrication strategy could be applicable to other metal nanoparticles anchored on graphene to form nanocomposites.

2. EXPERIMENTAL SECTION

2.1. Materials. Carbon black (VulcanXC-72) with a specific surface area (BET) of 250 m^2/g was purchased from Cabot. Natural graphite powder was obtained from Qingdao Ruisheng Graphite (purity 99.99%, particle size 40 μm). $H_2PtCl_6{\cdot}6H_2O$ was purchased from Aladdin Reagent. $RuCl_3$ was obtained from Sinopharm Chemical Reagent. Carbon dioxide was provided by Qingdao Heli Gas.

2.2. Synthesis of Graphene Sheets. Graphene sheets were synthesized according to the previously described method. GO[32,33] (0.8 g) (prepared by Hummers method[34,35]) was placed in a long quartz tube that was sealed at one end, and the other end was closed with a rubber stopper. Then, a nitrogen inlet was inserted through the rubber stopper. The sample was flushed with nitrogen for 5 min, and the quartz tube was quickly inserted into a muffle tube furnace preheated to 1050 °C and held in the furnace for a short time under nitrogen flow. According to the investigation of Schniepp et al.,[32,33] the surface area of dry graphene powder determined by the Brunauer−Emmett−Teller (BET) method was in the range of 600−1500 m^2/g but still lower than theoretical surface area of graphene (2630 m^2/g) because of the overlap of the exfoliated sheets.[32,33]

2.3. Synthesis of Pt/Graphene Composites. Pt/graphene composites were prepared using the experimental setup shown in Figure 1. In a typical experiment, 20 mg of graphene sheets and 20 mg of $Pt(acac)_2$ were ultrasonically dispersed in 5 mL of methanol. $Pt(acac)_2$ has a low solubility in SC CO_2. The addition of the methanol modifies the polarity of CO_2 and enables the dissolution of the Pt precursor in the fluid. Then, the suspension was loaded in a 25 mL stainless autoclave. The autoclave was sealed, and CO_2 was charged into the vessel up to desired pressure in an oven at 200 °C to obtain a SCF. Hydrogen gas of 1 MPa was initially filled in a H_2+CO_2 mixer cell, and CO_2 gas of 12 MPa was then added to the cell. After 1.5 h of waiting for the precursors to completely dissolve in the SC CO_2, the H_2+CO_2 gas was introduced into the reaction cell by pressurizing it to 16 MPa. The reduction (Pt^{2+} to Pt^0) occurred within tens of minutes. Then, the obtained mixture in the reaction cell was subjected to heat treatment in the H_2+CO_2 gas at 300 °C for 1.5 h. After the reaction cell was depressurized, Pt/graphene powders were collected, followed by sonication and washing five times using methanol. The produced sample was vacuum-dried at 60 °C for 6 h. Pt/CB composites were prepared following a similar experimental procedure.

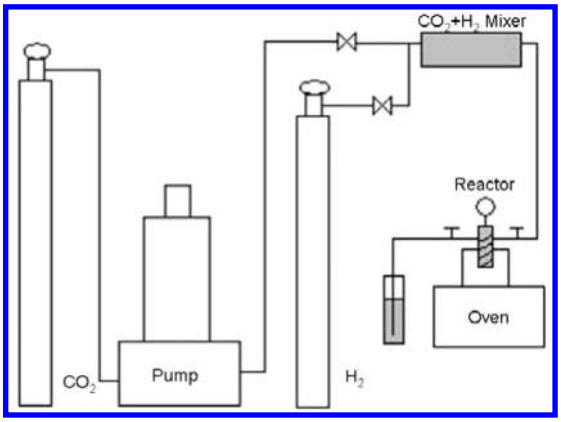

Figure 1. Experimental setup for the preparation of Pt/graphene in SC CO_2.

2.4. Electrocatalytic Activity Measurements. The electrochemical properties of the Pt/graphene and Pt/CB composites were evaluated by CV and CA tests using a conventional three-electrode cell on a CHI660B Electrochemical Workstation (Chenhua, China). All tests were conducted at room temperature. A glass carbon electrode coated with catalysts (3 mm in diameter) was used as the working electrode, a Pt wire as counter electrode, and Ag/AgCl electrode as reference electrode. 10 μL of *N*,*N*-dimethylformamide solution containing catalyst (2.5 mg/mL) was cast dropwise onto glass carbon electrode surface. After drying at room temperature in air, 8 μL of 0.05 wt % Nafion solution was dropped on the surface of the catalyst layer to form a thin film,

dx.doi.org/10.1021/jp3061976 | J. Phys. Chem. C 2012, 116, 21374−21381

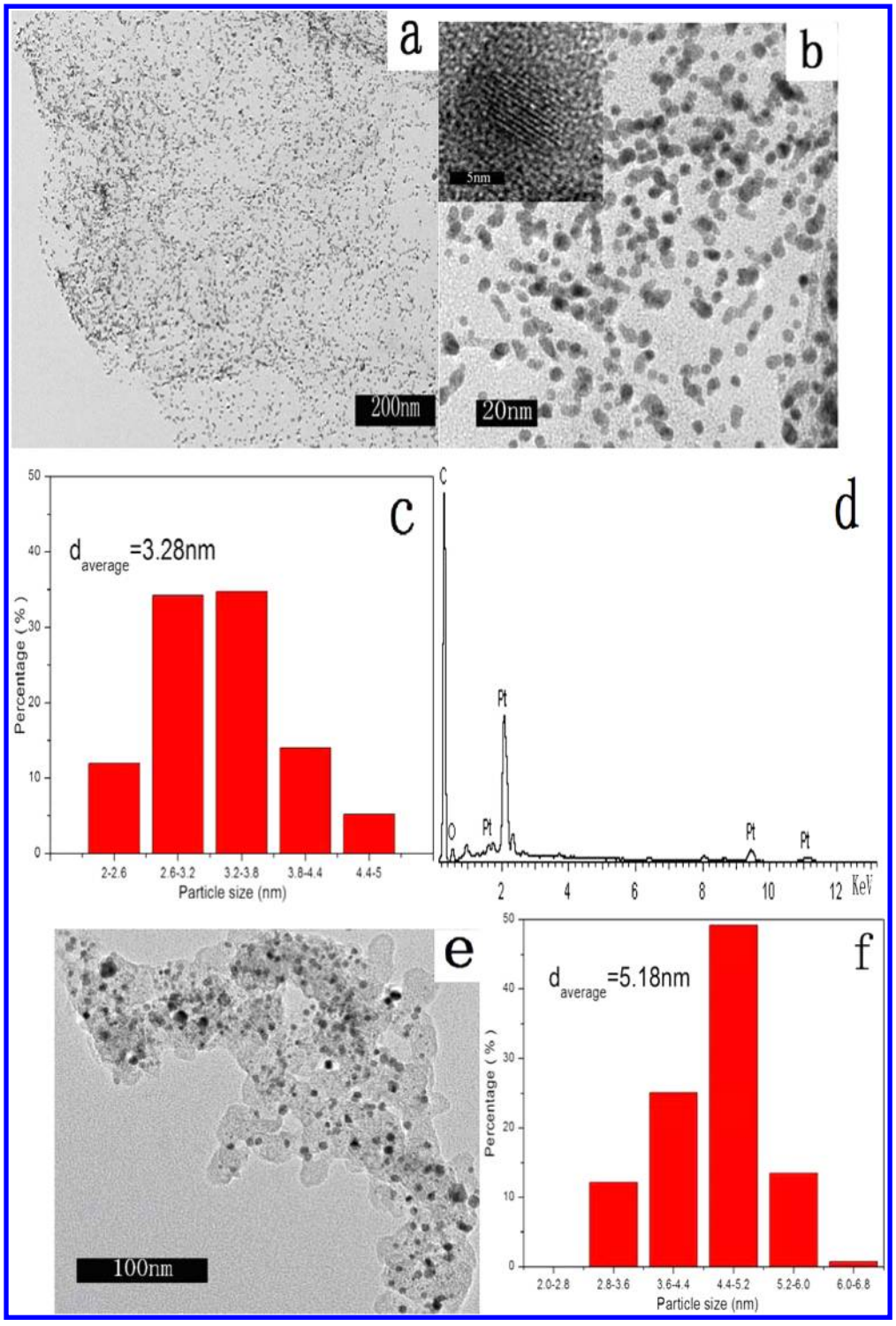

Figure 2. (a,b) Transmission electron microscopy (TEM) images of Pt/graphene, (c) the nanoparticle size distribution of Pt at graphene, (d) EDS spectra of Pt/graphene, (e) TEM image of Pt/carbon black (CB), and (f) the nanoparticle size distribution of Pt at carbon black (CB).

preventing catalyst from detaching. Prior to the electrochemical tests, the working electrode was dried for 3 h at room temperature.

Electrochemically active surface area (ECSA) of Pt nanoparticles was calculated from hydrogen electrosorption curve, which was recorded in 0.5 M H_2SO_4 solution. The electrocatalytic activity and stability of the synthesized Pt/graphene and Pt/CB for the oxidation of methanol were evaluated in 1 M CH_3OH and 0.5 M H_2SO_4 by means of CV and CA tests. The electrolyte solutions were deaerated with ultrahigh purity nitrogen for 15 min prior to any measurement.

2.5. Characterization. The composites were dispersed with 5 mL of HNO_3 and 5 mL of HCl in a hot block tube at 95 °C for 4 h. After being kept at room temperature overnight, 2 mL of HF was added to the sample solutions and dissolved at 95 °C for 2 h. The resulting solutions were analyzed by inductively coupled plasma spectroscopy/optical emission spectroscopy

dx.doi.org/10.1021/jp3061976 | J. Phys. Chem. C 2012, 116, 21374–21381

(ICP/OES, Perkin-Elmer, Optima 3300XL with AS 91auto-sampler) for the metal content of the prepared composites.

XRD patterns were obtained using a D-MAX 2500/PC operated at 40 kV and 100 mA with Cu Kα radiation (λ = 0.15418 nm). The XPS measurement of the composites was performed on a RBD upgraded PHI-5000C ESCA system (Perkin-Elmer) with Al Kα radiation ($h\nu$ = 1486.6 eV). The data analysis was carried out using RBD Augerscan 3.21 software (RBD Enterprises, USA). The morphologies of the products were examined by TEM on a JEOL 2010 transmission electron microscope equipped with an energy-dispersive X-ray spectrometer (EDS).

3. RESULTS AND DISCUSSION

3.1. Characterizations of Platinum Nanoparticles Deposited on Graphene Sheets. The TEM images of the as-prepared Pt/graphene composites are shown in Figure 2a,b. It can be clearly seen that the wrinkled graphene sheets were densely and uniformly coated by nanosized Pt particles with little aggregation. This is suggestive of a strong interaction between the graphene support and the Pt nanoparticles. The mean size of the Pt nanoparticles on graphene was estimated to be 3.28 nm (based on 200 particles) with a size distribution of 2.1−4.9 nm (Figure 2c). The Pt nanoparticles decorated on the graphene surfaces can act as "spacers" to prevent the graphene sheets from aggregation and restacking, making more surface area accessible. HRTEM image of individual Pt particles (Figure 2b) shows their single-crystalline structure with highly ordered, continuous fringe patterns. The measured interplanar spacing for the lattice fringes is 0.23 nm, which corresponds to the (111) lattice plane of face-centered cubic (fcc) Pt.

The homogeneous distribution of nanoparticles is associated with the role of SC CO_2. In our experiments, graphene sheets were first suspended in a methanol solution of platinum(II) acetylacetonate precursor. CO_2 was charged into the stainless-steel vessel, followed by the formation of a mixed SCF. Addition of the methanol modified the polarity of CO_2 and enabled the dissolution of the Pt precursor in the fluid. The graphene sheets could be wetted by metal precursors as a result of near-zero surface tension and high diffusivity of the SCF. Therefore, it facilitated the metal precursors to reach and be adsorbed on the surfaces of graphene sheets. The adsorbed precursors were then reduced by H_2 (hydrogen is well-dissolved in SC CO_2), followed by growing into nanoparticles.

The EDS spectrum of the Pt/graphene composites shows the peaks corresponding to Pt, C, and O elements, as illustrated in Figure 2d. For the purpose of comparison, we also deposited Pt nanoparticles on Vulcan XC-72 carbon black by using the SCF method under the same experimental conditions. As can be seen in Figure 2e, the Pt particle size on CB (average particle size, 5.18 nm with a size distribution of 2.8−6.4 nm in Figure 2f) is substantially larger than that on graphene, and their dispersion is much less uniform than that on graphene surfaces. Some nanoparticles are agglomerated (Figure 2e). The metal contents were estimated using inductively coupled plasma/optical emission spectroscopy (ICP/OES). The platinum loadings on graphene and carbon black are 23 and 22 wt %, respectively.

The XRD patterns of GO, graphene sheets and the as-synthesized Pt/graphene composite are displayed in Figure 3. The characteristic diffraction peak (0 0 2) of GO at 2θ = 11.1° corresponds to a d spacing of 0.80 nm (Figure 3a), which is due to the introduction of oxygenated functional groups such as

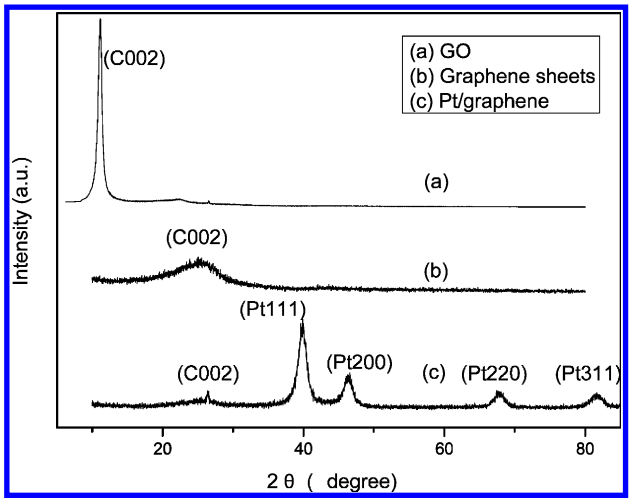

Figure 3. XRD patterns of (a) GO, (b) graphene sheets, (c) Pt/graphene.

epoxy (−O−), hydroxyl (−OH), and carboxyl (−COOH) groups. In the case of graphene (Figure 3b), the broad diffraction peak at 2θ = 26.5° is assigned to the C (0 0 2) reflections of the disorderedly stacked graphene sheets. That is, GO is partially reduced to graphene, and the sp^2-bonded graphene network was reestablished during the thermal reduction process. As shown in the XRD patterns of the nanocomposites (Figure 3c), the intensity of the (002) diffraction peak becomes weak because the restacking of graphene was inhibited by the attached Pt nanoparticles. Figure 3c also displays several peaks that correspond to the (111), (200), (220), and (311) facets of the face-centered cubic structures of Pt crystal, respectively. That is, the platinum precursor has been chemically reduced to metallic Pt nanoparticles by hydrogen.

The XPS analysis was performed on graphene and Pt/graphene. Figure 4a gives the survey XPS spectrum of the Pt/graphene composites. It could be clearly seen that C, O, and Pt exist in the composite, consistent with the EDS analysis. According to previous investigations,[22] the intensity of sp^2-hybridized C1s peak (284.5 eV) was significantly reduced after pure graphite was fully oxidized into GO, and additional peaks could be identified as oxygen-containing functional groups. After GO was reduced, the intensity of oxygen-containing groups dramatically decreased, indicating the reduction of GO and the restoration of the sp^2-hybridized graphene network. The C1s spectra of graphene and Pt/graphene are shown in Figure 4b,c. The high intensity of C−C bond (284.5 eV) indicates sp^2-conjugated carbon network. The presence of a small amount of oxygen-containing groups such as hydroxyl, epoxy and carboxyl groups on graphene sheets was detected[33] The spectrum of Pt 4f could be deconvoluted into three pairs of doublets (shown in Figure 4d). The strongest doublet coincides with peak binding energies of Pt 4f7/2 and 4f5/2 of Pt (0) at 71.2 and 74.6 eV, close to the values of Pt foil.[36] The two weaker doublets could be due to the slight oxidation of Pt nanoparticles upon exposure to air.[37] The doublets at 71.9 and 75.5 eV can be attributed to Pt(II) species such as PtO, and the broad doublets at 76.4 and 77.9 eV may be assigned to Pt(IV) species (PtO_2). The spectrum of Pt 4f suggests that metallic Pt (0) is the predominant species in the composites. The XPS analysis demonstrates that Pt/graphene composites were

dx.doi.org/10.1021/jp3061976 | J. Phys. Chem. C 2012, 116, 21374−21381

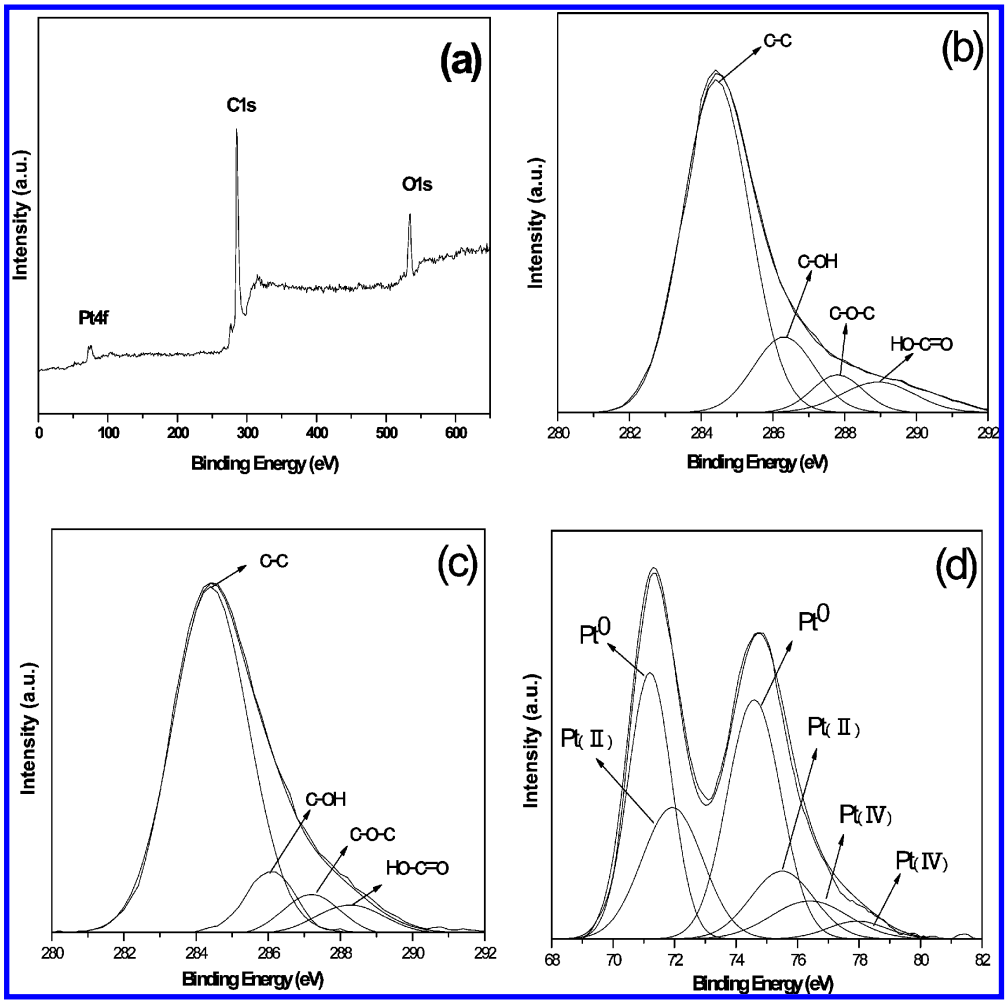

Figure 4. XPS spectra of the Pt/graphene composites: (a) the survey spectrum of Pt/graphene, (b) C1s spectrum of graphene, (c) C1s spectrum of Pt/graphene, and (d) Pt4f spectrum of Pt/graphene.

successfully prepared upon the hydrogen reduction of the precursor $Pt(acac)_2$ in the SCF.

Table 1 summarizes the deconvoluted peak positions and the areas relative to C1s sp^2 peak (expressed as a percentage).

Table 1. XPS Data of C1s of Graphene and Pt/Graphene Composites: Binding Energies and Relative Area Percentages with Respect to C−C Bonds in Parentheses

samples	C−C	C−OH	C−O−C	HO−C═O
graphene	284.4 (100)	286.3 (21)	287.8 (9)	288.9 (10)
Pt/graphene	284.4 (100)	286.1 (10)	287.2 (8)	288.3 (7)

Compared with graphene, it is evident that the intensities (relative amounts) of oxygenated functional groups decrease in the case of the Pt/graphene composites, indicating that graphene could be further reduced during the hydrogen reduction of the Pt organic precursor. Shenoy et al. recently reported that hydrogen treatment lead to more complete reduction of graphene oxide, and highly ordered ("graphitized") graphene can be obtained.[38] The XPS analysis (Table 1) indicates that hydroxyl (−OH) can be more easily removed during the hydrogen reduction process.

3.2. Electrochemical Characterization of the Pt/graphene Electrode. By using hydrogen adsorption−desorption methods in conjunction with CV, the ECSAs of the Pt/graphene and Pt/CB composites were measured. As shown in Figure 5, well-defined hydrogen adsorption/desorption characteristics are observed for both samples using CV in 0.5 M N_2-saturated H_2SO_4 solution. The ECSA can be

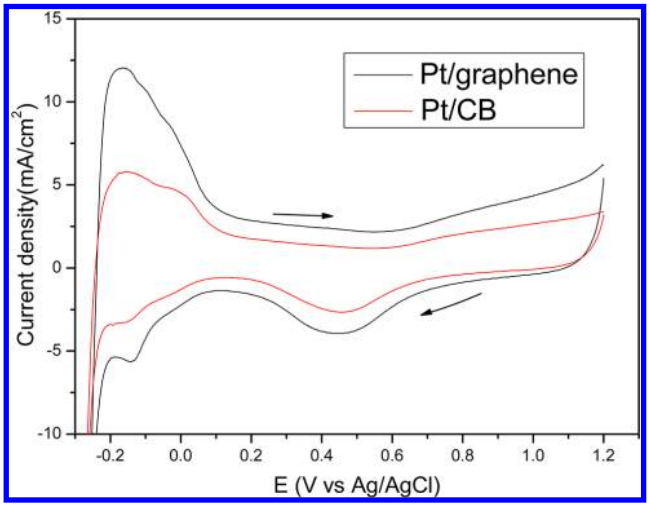

Figure 5. Cyclic voltammograms (CVs) at the Pt/carbon black (CB) and Pt/graphene electrodes in 0.5 M N_2-saturated H_2SO_4 solution at a scan rate of 50 mV/s.

dx.doi.org/10.1021/jp3061976 | J. Phys. Chem. C 2012, 116, 21374−21381

determined by the mean integral charge (Q_H) of the hydrogen adsorption and desorption area.[39,40]

It is found that the ECSA value of Pt/graphene (41.5 m^2/g) is much higher than the one obtained for Pt/CB (19.7 m^2/g), which can be ascribed to the smaller size of the Pt nanoparticles dispersed uniformly on the larger surface of graphene sheets. Additionally, the Pt nanoparticles dispersed on graphene surface could stop the restacking of graphene sheets, thus making many more Pt sites available on graphene surfaces for efficient catalytic activity. This ECSA analysis reveals that the Pt/graphene composites are electrochemically more accessible.

Methanol offers several advantages over hydrogen as a fuel including the ease of transportation and storage and high theoretical energy density. The methanol oxidation reaction occurs at the anode in DMFCs. Figure 6 compares cyclic

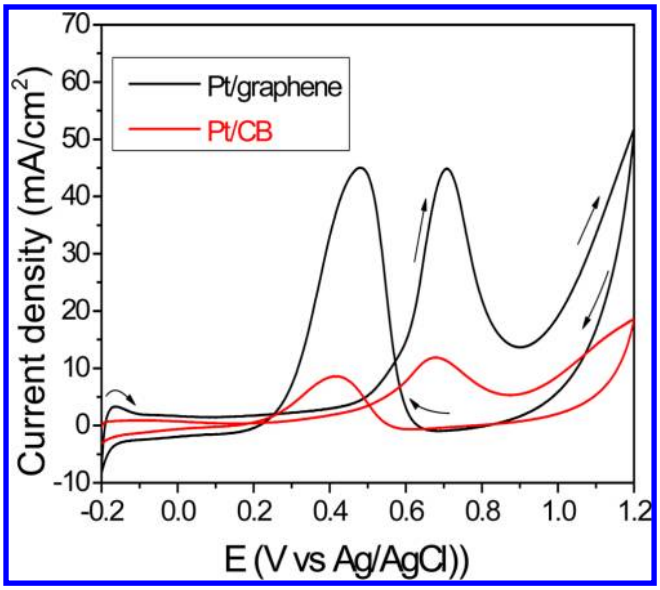

Figure 6. CVs of the Pt/carbon black (CB) and Pt/graphene electrodes in 0.5 M H_2SO_4 containing 1 M CH_3OH solution at a scan rate of 20 mV/s.

voltammograms (CVs) for electro-oxidation of methanol at the Pt/graphene and Pt/CB electrodes in 0.5 M H_2SO_4 containing 1 M CH_3OH solution at a scan rate of 20 mV/s. The stable voltammograms of electrodes were obtained after the fifth cycle. The electrocatalytic efficiencies of the Pt/graphene and Pt/CB composites for methanol oxidation are compared with regard to forward oxidation peak current density, mass activity, and onset potential. The relevant data are listed in Table 2.

For the methanol electro-oxidation by Pt catalyst, two oxidation peaks, which are related to the oxidation of methanol and the corresponding intermediates produced during the methanol oxidation, can be clearly observed. At the Pt/graphene electrode, the methanol oxidation peak current

Table 2. Comparison of the Electrocatalytic Parameters of Pt/Graphene and Pt/Carbon Black (CB) for Methanol Oxidation

samples	ECSA (m^2 g^{-1})	I_f (mA cm^{-2})	onset potential (V)	mass activity (mA/mg Pt)
Pt/graphene	41.5	44.8	0.17	550.4
Pt/CB	19.7	11.9	0.26	152.8

density (44.8 mA/cm^2) is found to be ~3.5 times higher than that of the Pt/CB electrode (11.9 mA/cm^2), revealing that Pt/graphene possesses a much better electrocatalytic activity for methanol oxidation than Pt/CB. The higher activity of the Pt/graphene catalyst may be a result of the larger specific surface of graphene, the smaller size of the Pt nanoparticles, and unique graphitic basal plane structure of graphene. (The effective restoration of sp^2-hybridized graphene network is needed.) The calculated mass activity (550.4 mA/mg Pt) of the Pt/graphene is higher than those of state-of-art Pt-based nanomaterials such as carbon nanofibers or CNTs-supported Pt nanoparticles,[41] CNTs/ionic liquid/Pt hybrids,[42] CNT/Pt composite catalysts[41,43] and polyaniline/Pt hybrid.[44] Meanwhile, the Pt/graphene composites prepared by this SCF method outperform many cases of recently reported graphene-based Pt nanoparticles in terms of mass activity.[45−47] Actually, to the best of our knowledge, the mass activity of the Pt/graphene catalyst is probably the best available value from various graphene-supported Pt particles. (Bimetallic particles are not included.)

In addition, it is notable that the onset potential of the Pt/graphene catalyst occurs at about 0.17 V, which is substantially lower than that (0.26 V) of the Pt/CB catalyst. The low onset potential presents clear evidence for excellent electrocatalytic activity for methanol oxidation.

Furthermore, the stabilities of the Pt/graphene and Pt/CB electrodes were measured by CA. The corresponding *i*−*t* curve is shown in Figure 7. It can be clearly seen that the current

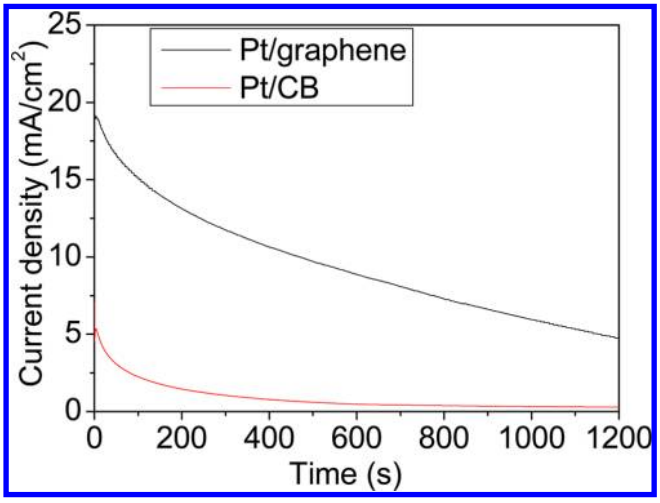

Figure 7. *I*−*t* curves of the Pt/graphene and Pt/carbon black (CB) electrodes at 0.6 V for 1200 s in the mix solution of 1 M CH_3OH and 0.5 M H_2SO_4 solution saturated by N_2 at room temperature.

density decay of the Pt/graphene catalyst is slower than the Pt/CB catalyst in the initial period, and the current density of the Pt/graphene electrode is considerably higher than that of the Pt/CB electrode during the whole time. The result implies that as compared with the Pt/CB catalyst, the Pt/graphene catalyst possesses significantly improved electrocatalytic activity and stability for methanol oxidation.

The employment of graphene and the SCF-assisted fabrication of the Pt/graphene catalyst are demonstrated to improve significantly the catalytic activity and stability for methanol oxidation as compared with their carbon black counterparts. The graphene sheets as a highly conductive 2-D carbon carrier possess larger surface area and enable more

dx.doi.org/10.1021/jp3061976 | J. Phys. Chem. C 2012, 116, 21374−21381

uniform dispersion of metallic nanoparticles than the conventional carbon support carbon black (Vulcan XC-72). As a consequence, more Pt surface sites are accessible on effectively graphitized graphene sheets for methanol oxidation.

4. CONCLUSIONS

In conclusion, we report a facile and effective SCF approach to load Pt nanoparticles on graphene sheets. The unique properties of SCFs lead to the uniform deposition of metal catalysts on the graphene surface. Remarkable enhancements in electrocatalytic activities and stability for methanol oxidation are obtained in the Pt/graphene composites, as compared with Pt/carbon black composites. These results demonstrate that the use of SCF is a viable method for preparing graphene-based metallic composites and can be readily used to synthesize other metal or alloy particle-based hybrids. Graphene can serve a favorable candidate as a supporting material of electrocatalysts, and the resultant Pt/graphene composites fabricated in SC CO_2 show a great promise for the development of high electroactive catalysts for fuel cells.

AUTHOR INFORMATION

Corresponding Author

*Tel/Fax: +86 0532 84022725. E-mail: Jian.Zhao2010@gmail.com.

Notes

The authors declare no competing financial interest.

ACKNOWLEDGMENTS

The work was partially funded by the National Natural Science Foundation of China (Nos. 21173190, 51073082, and 50943026), the International Science and Technology Cooperation Program of China (2012DFG42100), the Doctoral Program of Higher Education of China (2011010113003), the Scientific Research Foundation for the Returned Overseas Chinese Scholars, Qingdao Municipal Science and Technology Program, Basic Research Project (12-1-4-3-(7)-jch and 12-1-4-3-(25)-jch), Chongqing Key Laboratory of Micro/Nano Materials Engineering and Technology (open project KFJJ1202), MOE Key Laboratory of Organosilicon Chemistry and Material Technology of Ministry of Education (open project YJG2010-02) (Hangzhou Normal University), State Key Laboratory of Chemical Resource Engineering (open project CRE-2012-C-204) (Beijing University of Chemical Engineering), MOE Key Laboratory of Molecular Engineering of Polymers (Fudan University), and the natural science foundation of Shandong Province (ZR2012EMM003).

REFERENCES

(1) Chan, K.-Y.; Ding, J.; Ren, J.; Cheng, S.; Tsang, K. Y. *J. Mater. Chem.* **2004**, *14*, 505−516.
(2) Olah, G. A. *Angew. Chem., Int. Ed.* **2005**, *44*, 2636−2639.
(3) Dong, L.; Liu, Q.; Wang, L.; Chen, K. *Physics and Applications of Graphene - Experiments*; InTEch: Rijeka, Croatia, 2011; pp 525−540.
(4) Haggin, J. *Chem. Eng. News* **1995**, *73*, 8.
(5) Shimizu, K.; Wang, J. S.; Wai, C. M. *J. Phys. Chem. A* **2009**, *114*, 3956−3961.
(6) Aricò, A. S.; Baglio, V.; Antonucci, V. Direct Methanol Fuel Cells: History, Status and Perspectives. In *Electrocatalysis of Direct Methanol Fuel Cells*; Wiley-VCH Verlag: Weinheim, Germany, 2009; pp 1−78.
(7) Sandstede, G.; Cairns, E. J.; Bagotsky, V. S.; Wiesener, K. History of Low Temperature Fuel Cells. In *Handbook of Fuel Cells*; John Wiley & Sons, Ltd.: NJ, 2010.
(8) Scott, K.; Yu, E. Electrocatalysis in the Direct Methanol Alkaline Fuel Cell. In *Electrocatalysis of Direct Methanol Fuel Cells*; Liu, H., Zhang, J., Eds.; Wiley-VCH Verlag: Weinheim, Germany, 2009; pp 487−525.
(9) Rathod, D.; Dickinson, C.; Egan, D.; Dempsey, E. *Sens. Actuators, B* **2010**, *143*, 547−554.
(10) Xu, W.; Lu, T.; Liu, C.; Xing, W. *J. Phys. Chem. B* **2005**, *109*, 14325−14330.
(11) Lin, Y.; Cui, X. *J. Phys. Chem. B* **2005**, *109*, 14410−14415.
(12) Geim, A. K.; Novoselov, K. S. *Nat. Mater.* **2007**, *6*, 183−191.
(13) Zhu, J. *Nat. Nanotechnol* **2008**, *3*, 528−529.
(14) Li, D.; Kaner, R. B. *Science* **2008**, *320*, 1170−1171.
(15) Stankovich, S.; Dikin, D. A.; Dommett, D.; Kohlhaas, K.; Zimney, E.; Stach, E. *Nature* **2006**, *442*, 282−286.
(16) Qiu, J.; Wang, G.; Liang, R.; Xia, X.; Yu, H. *J. Phys. Chem. C* **2011**, *115*, 15639−15645.
(17) Yen, M.-Y.; Teng, C.-C.; Hsiao, M.-C.; Liu, P.-I.; Chuang, W.-P.; Ma, C.-C. M.; Hsieh, C.-K.; Tsai, M.-C.; tsai, C.-H. *J. Mater. Chem.* **2011**, *21*, 12880−12888.
(18) Shao, Y.; Zhang, S.; Wang, C.; Nie, Z.; Liu, J.; Wang, Y.; Lin, Y. *J. Power Sources* **2010**, *195*, 4600−4605.
(19) Shafiei, M.; Spizzirri, P. G.; Arsat, R.; Yu, J.; du Plessis, J.; Dubin, S.; Kaner, R. B.; Kalantar-zadeh, K.; Wlodarski, W. *J. Phys. Chem. C* **2010**, *114*, 13796−13801.
(20) Nethravathi, C.; Anumol, E. A.; Rajamathi, M.; Ravishankar, N. *Nanoscale* **2010**, *3*, 569−571.
(21) Liu, S.; Wang, J.; Zeng, J.; Ou, J.; Li, Z.; Liu, X.; Yang, S. *J. Power Sources* **2010**, *195*, 4628−4633.
(22) Li, Y.; Gao, W.; Ci, L.; Wang, C.; Ajayan, P. M. *Carbon* **2010**, *48*, 1124−1130.
(23) Dong, L.; Gari, R. R. S.; Li, Z.; Craig, M. M.; Hou, S. *Carbon* **2010**, *48*, 781−787.
(24) Si, Y.; Samulski, E. T. *Nano Lett.* **2008**, *8*, 1679−1682.
(25) Li, Y.; Fan, X.; Qi, J.; Ji, J.; Wang, S.; Zhang, G.; Zhang, F. *Mater. Res. Bull.* **2010**, *45*, 1413−1418.
(26) Guo, S.; Dong, S.; Wang, E. *ACS Nano* **2009**, *4*, 547−555.
(27) Si, Y.; Samulski, E. T. *Chem. Mater.* **2008**, *20*, 6792−6797.
(28) Ye, X.-R.; Lin, Y.; Wang, C.; Engelhard, M. H.; Wang, Y.; Wai, C. M. *J. Mater. Chem.* **2004**, *14*, 908−913.
(29) Lin, Y.; Cui, X.; Yen, C. H.; Wai, C. M. *Langmuir* **2005**, *21*, 11474−11479.
(30) Sun, Z.; Liu, Z.; Han, B.; Miao, S.; Miao, Z.; An, G. *J. Colloid Interface Sci.* **2006**, *304*, 323−328.
(31) An, G.; Yu, P.; Mao, L.; Sun, Z.; Liu, Z.; Miao, S.; Miao, Z.; Ding, K. *Carbon* **2007**, *45*, 536−542.
(32) McAllister, M. J.; Li, J.-L.; Adamson, D. H.; Schniepp, H. C.; Abdala, A. A.; Liu, J.; Herrera-Alonso, M.; Milius, D. L.; Car, R.; Prud'homme, R. K.; Aksay, I. A. *Chem. Mater.* **2007**, *19*, 4396−4404.
(33) Schniepp, H. C.; Li, J.-L.; McAllister, M. J.; Sai, H.; Herrera-Alonso, M.; Adamson, D. H.; Prud'homme, R. K.; Car, R.; Saville, D. A.; Aksay, I. A. *J. Phys. Chem. B* **2006**, *110*, 8535−8539.
(34) Becerril, H. A.; Mao, J.; Liu, Z.; Stoltenberg, R. M.; Bao, Z.; Chen, Y. *ACS Nano* **2008**, *2*, 463−470.
(35) Hummers, W. S.; Offeman, R. E. *J. Am. Chem. Soc.* **1958**, *80*, 1339−1339.
(36) Bonet, F.; Delmas, V.; Grugeon, S.; Herrera Urbina, R.; Silvert, P. Y.; Tekaia-Elhsissen, K. *Nanostruct. Mater.* **1999**, *11*, 1277−1284.
(37) T, F.; W, V.; AP, C.; JAR., V. *Electrochim. Acta* **1995**, *40*, 1537−1543.
(38) Bagri, A.; Mattevi, C.; Acik, M.; Chabal, Y. J.; Chhowalla, M.; Shenoy, V. B. *Nat. Chem.* **2010**, *2*, 581−587.
(39) Girishkumar, G.; Rettker, M.; Underhile, R.; Binz, D.; Vinodgopal, K.; McGinn, P.; Kamat, P. *Langmuir* **2005**, *21*, 8487−8494.
(40) Pozio, A.; De Francesco, M.; Cemmi, A.; Cardellini, F.; Giorgi, L. *J. Power Sources* **2002**, *105*, 13−19.
(41) Hsin, Y. L.; Hwang, K. C.; Yeh, C.-T. *J. Am. Chem. Soc.* **2007**, *129*, 9999−10010.

(42) Wu, B.; Hu, D.; Kuang, Y.; Liu, B.; Zhang, X.; Chen, J. *Angew. Chem., Int. Ed.* **2009**, *48*, 4751−4754.
(43) Mu, Y.; Liang, H.; Hu, J.; Jiang, L.; Wan, L. *J. Phys. Chem. B* **2005**, *109*, 22212−22216.
(44) Guo, S.; Dong, S.; Wang, E. *Small* **2009**, *5*, 1869−1876.
(45) Li, Y.; Tang, L.; Li, J. *Electrochem. Commun.* **2009**, *11*, 846−849.
(46) Nethravathi, C.; Anumol, E. A.; Rajamathi, M.; Ravishankar, N. *Nanoscale* **2011**, *3*, 569−571.
(47) Zhou, Y.; Chen, J.; Wang, F.; Sheng, Z.; Xia, X. *Chem. Commun.* **2010**, *2010*, 5951−5953.